DOI: 10.13009/EUCASS2023-012
Aerospace Europe Conference 2023 – 10TH EUCASS – 9TH CEAS

Design Optimisation of Hybrid Propellant Sounding Rockets

Allen Chan⋆, *Mitchell Galletly*⋆† *and Dries Verstraete*⋆
⋆*University of Sydney*
Sydney, Australia
acha7851@uni.sydney.edu.au · mitchell.galletly@sydney.edu.au · dries.verstraete@sydney.edu.au
†Corresponding author

Abstract

With the recently renewed interest in hybrid propulsion systems, there is a growing need for a vehicle design optimisation toolbox. This paper presents a multidisciplinary design optimisation framework using a Non-Dominated Sorting Genetic Algorithm (NSGA-II) to determine the ideal vehicle design for a given mission profile. The conceptual design of a 100 km experimental sounding rocket is developed using this framework. The derived vehicle designs are examined in detail to assess the effectiveness of the design tool. The optimiser produced vehicles very similar in size to existing flight-proven vehicles, confirming that the results are credible. The study also demonstrated the effect of the choice of propellant and fuel grain geometry on the overall vehicle design.

1. Introduction

Hybrid propulsion systems provide a promising alternative for current launch vehicles. As a result, the technology has recently gained momentum, with the concept being adopted by many research institutions and start-up launch providers.[1–3] In light of these recent endeavours, this paper presents a vehicle design optimisation toolbox to facilitate the design and development of hybrid propellant launch vehicles. Vehicle design and sizing is a highly iterative and cyclic process requiring extensive trade-off studies between aerodynamics, structures, propulsion, mass, and trajectory. This complex process requires compromises between individual subsystems and mission objectives, necessitating design optimisation to provide a more cohesive and effective design tool for launch vehicle development. However, to date, minimal progress has been made in developing medium to high-fidelity design optimisation tools for large design domains. Many existing tools implement a low-fidelity approach, and this study aims to address this knowledge gap and provide insight into the ideal design choices for hybrid sounding rockets.

Multi-disciplinary and multi-objective design optimisation techniques have been applied to a range of hybrid engine powered vehicles ranging from experimental sounding ground-launched[4–7] and air-launched rockets[6] through to orbital[8] and re-entry vehicles.[9] Many of the previous studies that examine the full-flight vehicle use a low-fidelity approach with highly simplified assumptions to model the vehicle dynamics and engine aerothermodynamics. Some of the main underlying simplifications include: implementing only a 2 degree of freedom (2-DOF) flight trajectory simulation with approximated aerodynamic coefficients,[7] using low order analytical regression rate models,[10] chemical equilibrium evaluations calculated only at stoichiometric ratios which do not consider the transient effects of the motor burn,[6] and ideal isentropic equations which do not take into account the losses incurred by combustion inefficiencies and nozzle geometries.[5] Zhu et al. performed a more comprehensive design optimisation study for staged low Earth orbit (LEO) launch vehicles but only used a 3-DOF simulation and approximated the aerodynamic coefficients using an existing similar-sized rocket.[7] Although these simplified models provide a good starting point to develop the vehicle, a higher fidelity model will offer a more cohesive and realistic representation of the selected design. Higher fidelity models incorporating transient effects of the motor burn were implemented in many fuel grain and engine optimisations efforts;[4,11,12] however, these had little to no regard for the vehicle's design.

In 1998, Anderson[13] created an objective function and genetic algorithm for the design optimisation of single-stage solid propellant vehicles.[14] The software incorporated a full 6-degree of freedom (6-DOF) trajectory simulator, mass prediction, aerodynamics, and propulsion model. Since then, other authors have continuously extended the work in this area. A review conducted by Mahjub et al. found that genetic algorithms were the most widely used tool for the design optimisation of solid rocket motors.[15] Similarly, this trend is reflected in most of the limited literature on hybrid launch vehicle design optimisation. Casalino et al. implemented a cooperative evolutionary algorithm employing a genetic algorithm, differential evolution, and particle swarm optimisation in parallel to derive the optimal engine design for a range of propellant combinations.[4] The approach found near-optimal solutions with a reduced run time compared

DOI: 10.13009/EUCASS2023-012

to more popular methods.[4] Burak et al.[5] and Kaled et al.[9] also implemented various genetic algorithms to design a hybrid engine; however, both used a very low-fidelity vehicle dynamic and engine ballistic model. Leverone conducted an extensive set of manual parametric design studies using a high-fidelity hybrid rocket simulation tool developed by the University of KwaZulu-Nata to optimise the design of a 100 km N_2O/paraffin propellant vehicle[16] and this approach could have significantly benefited from an optimisation algorithm instead.

This paper presents a design optimisation framework for developing hybrid propellant launch vehicles. The software suite is centralised around a medium-fidelity simulation toolbox and aims to address the shortcomings of current optimisation approaches. The work focuses on developing sub-orbital sounding rockets; however, the software is designed to be extensible such that a range of vehicle classes can be included with additional functionality. This paper covers the simulation models and methods used for developing the design optimisation framework. Comparison with existing test firing and flight data is used to validate the models. The framework is used to design a 100 km apogee sounding rocket and an assessment of the validity of the design is presented.

2. Simulation Models and Methods

The vehicle design optimisation environment comprises a set of interconnected modules developed in Python using object-oriented programming. This modular approach allows for a flexible design environment where individual sub-components can be interchanged with alternative simulation approaches or higher fidelity methods. It allows the entire software suite to be extended to accommodate additional functionality. The design toolbox is also interfaced with external simulation code and open-source Python libraries to assist with the modelling and optimisation procedure.

The design toolbox comprises three main modules: an optimiser, a material and propellant database, and a performance analysis framework, as shown in Figure 1. The performance analysis module is the main element and features integrated aerodynamics, weight estimation, propulsion, and trajectory sub-modules to size the vehicle and model the full flight performance of the proposed design. In addition, the mechanical properties of materials and the chemical properties of propellants are supplied from a database to allow evaluation of a range of design options. Finally, this is interfaced with an optimisation framework that feeds design inputs into the performance analysis module and assesses the vehicle's performance to the mission objectives and constraints. This process is conducted in a design loop and continually iterates until an optimal solution is derived. A high-level overview of the system architecture and the interaction between individual sub-modules and external libraries is shown in Figure 1, and a detailed discussion of the methodology is given in the following sections.

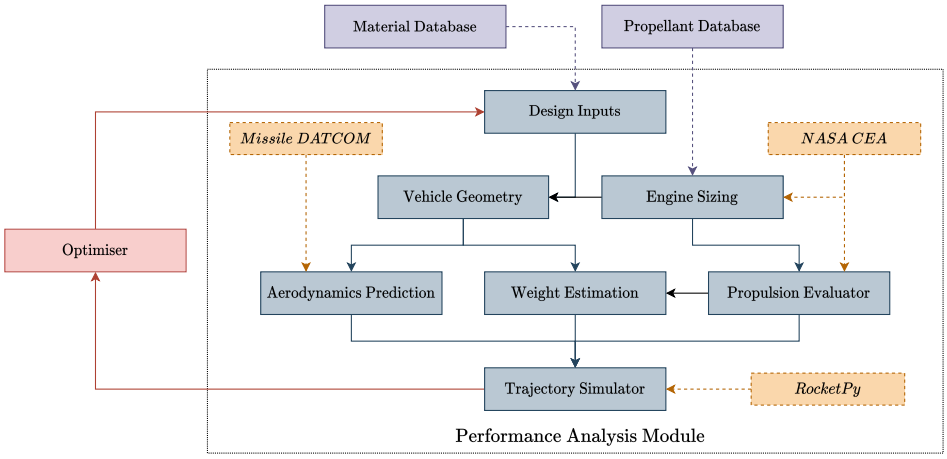

Figure 1: Software architecture showing interaction between sub-modules.

2.1 Propulsion

Design and evaluation of the propulsion system is conducted using the engine sizing and analysis tool. This tool is comprised of two sub-modules: an engine sizing function and a performance evaluator. The engine performance target metrics are initially fed into the engine sizing module, which determines the engine design specifications for a single design point. This design is then passed to a performance evaluator to simulate the complete transient burn profile of the engine. As shown in Figure 1, both modules are interfaced with NASA's Chemical Equilibrium and Applications (CEA).[17,18]

DOI: 10.13009/EUCASS2023-012

2.1.1 Engine Sizing

The engine sizing tool derives all the design parameters required to completely define the propulsion system at a preliminary level, including specifications for the oxidiser tank, combustion chamber, fuel grain, and nozzle. The calculation requires the target thrust F_{opt}, burn time t_b, chamber pressure P_c, tank pressure P_t, target oxidiser to fuel ratio OF, ambient operating conditions T_{amb} and P_{amb} as well as the feed system parameters to be defined. An overview of the design process and the input/output of each sizing function is provided in Figure 2. This design process is an extension of the design procedure outlined by Humble et al.[19]

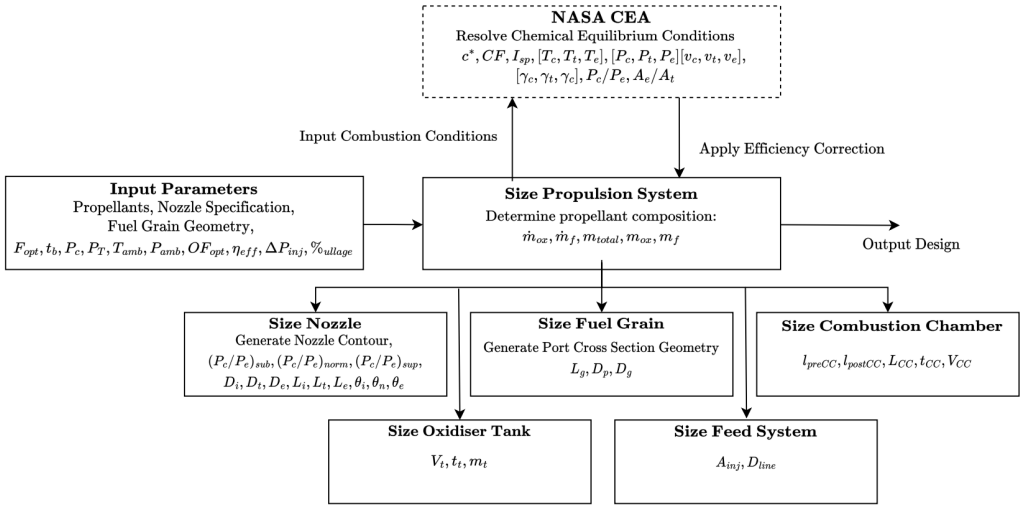

Figure 2: Overview of engine sizing process and function interactions.

2.1.2 Engine Performance

The performance evaluation module models the motor's complete transient burn profile, simulating the oxidiser tank's self-pressurisation and blow-down dynamics combined with internal ballistics, fuel regression, and nozzle flow model for accurate predictions of the overall engine performance. This model is developed using a control volume approach by dividing the propulsion system into three sections encompassing the oxidiser tank, the combustion chamber, and the nozzle, as shown in Figure 3.

A mass and energy balance is conducted to derive the set of differential equations used to describe the dynamics of each subsystem, and a time-marching numerical integration scheme is used to resolve the properties. For a given time-step, each segment is independently resolved and then coupled to derive the complete operational performance profile. Using this approach, the thrust curve, impulse, change in propellant mass, and internal chamber properties can be accurately predicted. The numerical approach used in this model was adapted from the works of Genévivie et al.[20,21] Since nitrous oxide is primarily used in this study, the oxidiser feed system is simulated using a model developed by Borgdorff[22] with good agreement compared to experimental testing. By applying the first law of thermodynamics, considering the change of enthalpy within the system along with the conservation of mass, the change in chamber pressure can be expressed as:[20]

$$\frac{dP_c}{dt} = \frac{\gamma_c - 1}{V_c}\left[\left(c_{p_c}T_c\right)\left(\frac{dm_{ox}}{dt} + \frac{dm_f}{dt}\right) - \left(c_{p_{noz}}T_{noz}\right)\frac{dm_{noz}}{dt}\right] - \left[\frac{\gamma_c P_c}{V_c}\right]\frac{dV_c}{dt} + \left[\frac{P_c}{V_c - 1}\right]\frac{d\gamma_c}{dt} \tag{1}$$

Here V_c is the chamber volume, $\frac{dm_{ox}}{dt}$ and $\frac{dm_f}{dt}$ represent the fuel and oxidiser mass flow rate into the system, $\frac{dm_{noz}}{dt}$ is the combustion gases exiting the system into the nozzle, c_p is the specific heat capacity of the propellant combination, γ is the ratio of specific heats, and T is the temperature. The modelling technique has been used by McCulley et al.[23] and Chelaru et al.;[24] however, a complete derivation of the equation is provided by Genévivie.[20] The oxidiser mass flow rate $\frac{dm_{ox}}{dt}$ is provided by CV_1. By considering the fuel geometry and applying the classical Marxman's fuel regression equation,[25] the volume differential $\frac{dV_c}{dt}$, and fuel mass flow rate $\frac{dm_f}{dt}$ can be determined:

$$\dot{r} = aG_{ox}^n \tag{2}$$

DOI: 10.13009/EUCASS2023-012

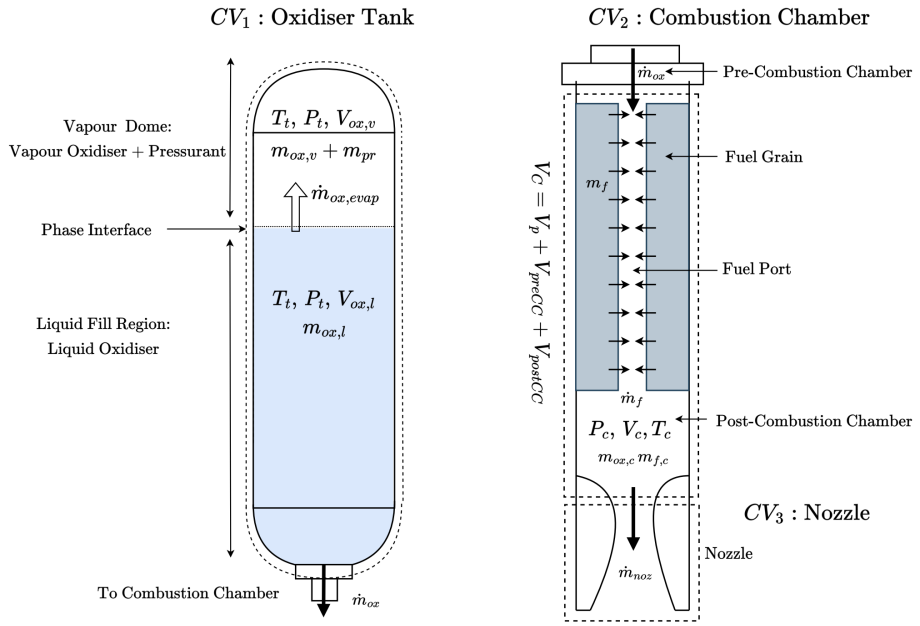

Figure 3: Schematic diagram of control volume approach.

$$\frac{dV_c}{dt} = p_p L_g \dot{r} \tag{3}$$

$$\frac{dm_f}{dt} = p_p L_g \rho_f \dot{r} \tag{4}$$

The system OF ratio can be determined by the unburnt propellant within the chamber:

$$OF = \frac{m_{ox,c} + \left[\frac{dm_{ox}}{dt} - \frac{dm_{noz}}{dt}\left(\frac{OF}{OF+1}\right)\right]\Delta t}{m_{f,c} + \left[\frac{dm_f}{dt} - \frac{dm_{noz}}{dt}\left(\frac{1}{OF+1}\right)\right]\Delta t} \tag{5}$$

With the pressure and propellant ratio defined, CEA is called to compute combustion thermodynamics and transport properties, assuming a finite area combustor. CEA also provides the heat capacity values to resolve Equation 1 and $\frac{d\gamma_c}{dt}$ is approximated using a backwards difference temporal discretisation scheme extracted from CEA outputs. Like CV_1, an Euler time integration scheme resolves Equation 1 and determines the transient chamber properties. This control volume provides all the information necessary to compute the nozzle flow and determine the engine performance.

2.2 Weight and Structures

Precise weight estimations are required to model the flight dynamics of the vehicle accurately. Weight estimation is also vital for optimisation cases as most problems are defined to minimise overall vehicle mass or the payload mass ratio. The weight estimation module developed in this code estimates the vehicle's total mass, the centre of gravity, moments of inertia and the time-dependent change of these properties as the propellant is consumed. A component build-up approach is used where the weights and inertias are individually calculated on a subsystem basis. The method combines empirical techniques with analytical approaches for structural sizing and is linked to a material properties database.[26] Weight estimation requires design inputs to be specified; this includes the subsystem layout, airframe geometries, materials used and the factor of safety for structural components. By taking this approach, an accurate prediction can be determined for a broader range of vehicle designs. The implementation only considers single-staged vehicles; however, the framework can be extended to multi-stage configurations.

2.3 Aerodynamics

The aerodynamics module predicts the aerodynamic forces and moments that act on the vehicle throughout its flight. These are calculated as part of the trajectory simulator; however, the vehicle's aerodynamic coefficients and stability derivatives are estimated using Missile DATCOM. The U.S. Airforce Missile DATCOM code is a comprehensive

DOI: 10.13009/EUCASS2023-012

semi-empirical datasheet component build-up method used for the preliminary design and analysis of axisymmetric and non-axisymmetric missiles and sounding rockets.[27] The component build-up approach provides higher flexibility, allowing for a range of conventional vehicle geometries to be defined and evaluated at a low computational expense without resorting to higher fidelity methods such as panel codes or CFD.

DATCOM resolves the aerodynamics coefficients and stability derivatives for a defined range of discrete Mach Numbers M and angle of attacks α. A wrapper translates the vehicle geometry into a DATCOM input file with defined flight conditions (altitude, Mach Number range, angle of attack range). An output file containing all the aerodynamic parameters is then read in, and a lookup table is created using a linear interpolation scheme.

2.4 Trajectory

With the vehicle specifications completely defined, the vehicle is passed into a trajectory simulator where flight dynamics of the rocket's ascent are modelled. A 6-DOF simulator is selected as it provides a more accurate representation of the vehicle's flight profile and overall performance. A range of ballistic trajectory simulation codes was assessed, and RocketPy was selected for this analysis. RocketPy is an open-source Python library developed by The University of São Paulo specifically for the analysis of sounding rockets.[28] The toolbox offers the ability to configure custom-designed rockets with interchangeable propulsion systems, an environment class with an International Standard Atmosphere model and live weather forecast, as well as a Monte Carlo analysis tool for statistical estimates of key flight outputs to model uncertainties in weather.[28] The software architecture is structured in such a way that modifications to the code can easily be implemented.

RocketPy was developed for the analysis of solid propellant vehicles. The code was modified to cater to hybrid propulsion systems by replacing functions that model the thrust profile, propellant mass change and CG shift with outputs from the propulsion and weight estimation toolbox. The aerodynamic forces in the original code were calculated from coefficients extracted from an input file and this is replaced with a look-up table function passed in from the aerodynamics module. The trajectory simulator incorporates all flight phases necessary for this analysis, including launch rail-guided ascent, 6-DOF flight, and 3-DOF parachute descent. The simulator employs the standard six degrees of motion equations with additional terms for jet dampening[29] and variable mass effects[30] to achieve a higher order of accuracy. An LSODA numerical scheme is used to perform the time integration of the equations of motion.

2.5 Design Optimisation

Multi-Disciplinary Design Optimisation is achieved using a Non-Dominated Sorting Genetic Algorithm (NSGA-II).[31] Genetic algorithms have proven effective in optimising various engineering design problems, especially in aerospace vehicle development, where optimisation is a critical element of the design process.[32] Genetic algorithms are more suitable for engineering design problems as they explore an extensive search space and are more likely to converge to a globally optimal solution than particle swarm and binary descent algorithms.[33] An objective function integrates the design and performance analysis module with the optimiser. The objective function takes in an array of input parameters and calculates metrics that the optimiser seeks to minimise or maximise. In this implementation, design parameters defining the vehicle are fed into the objective function, where the vehicle is created and then evaluated. Selected performance parameters of interest are then returned from the function and used as the basis for optimisation. In addition, constraints are also put in place to ensure non-physical solutions or infeasible designs are filtered out of the population.

3. Model Validation

The performance analysis models are validated against available experimental data. Due to the novelty of hybrid launch vehicles, published data encompassing vehicle design specifications, static firing data, and test flight data are scarce. As a result, a complete study comparing three vehicles of varying scales is presented here. The three vehicles investigated all exhibited nominal flight sequences, and these include:

- **Unexploded Ordnance (UXO) - University of Waterloo (2018):** Unexploded Ordnance was Waterloo Rocketry's 2018 entry into the Intercollegiate Rocket Engineering Competition (IREC) for Student Research and Developed (SRAD) hybrid vehicles. The vehicle was initially designed for the 30,000 ft category; however, it was scaled back to a 10,000 ft target apogee due to poor combustion efficiencies observed during testing.[34]
- **Phoenix P1B - University of KwaZulu-Natal (2021):** P1B is the second series of sounding rockets developed by the University of KwaZulu-Natal to address the lack of indigenous sub-orbital launch capabilities in South

DOI: 10.13009/EUCASS2023-012

Africa. The program aims to develop a cost-effective platform for high-altitude scientific research. The vehicle was successfully launched in 2021, reaching an altitude of 17.9 km.[35,36]

– **HEROS 3 - HyEND University of Stuttgart (2017):** HEROS 3 was developed in collaboration with the German Aerospace Research Center (DLR). In 2017, the team broke the altitude record for European student and amateur rocketry, reaching an apogee of 32.3 km.[37,38]

3.1 Engine Performance Modelling

The propulsion module is validated against static test-firing data provided in the reports of all three vehicles assessed. Engine operating targets from each vehicle were fed into the engine design module. The design specifications derived by the sizing function showed good agreement with the actual design of each given engine. Margins of error between 5-30 % for the propellant mass requirements, engine dimensions, and expected operating conditions were observed. More significant errors are expected to some degree, as the actual engine would have undergone multiple design iterations to optimise performance and this process is not reflected in the sizing code. On the other hand, the performance analysis model uses exact engine details provided by the reports to generate the following results instead of the engine details predicted by the engine design module. Figures 4-6 compare the simulated performances and recorded test data. Here, the thrust, chamber, and tank pressure are compared, as these are the most important quantities governing the engine's performance.

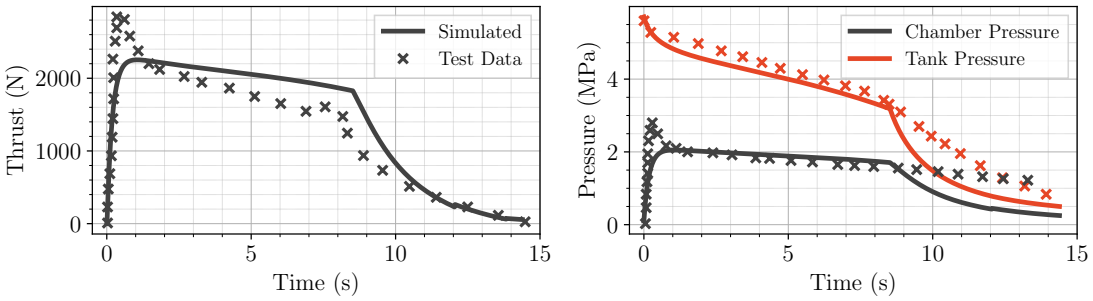

Figure 4: Validation of engine performance model against UXO's Kismet Hybrid Engine test fire data.[34]

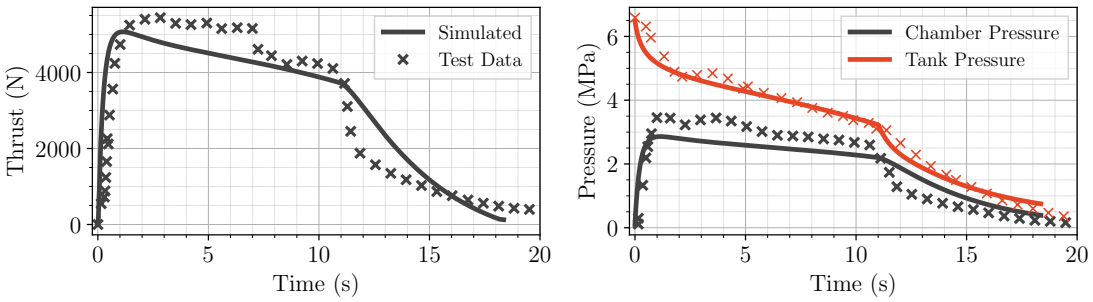

Figure 5: Validation of engine performance model against P1B-Mk's test fire data.[36]

All cases align relatively well against the experimental data, with some discrepancies. As seen in Figure 4, the Kismet engine initially exhibits a sharp spike during the start-up phase, indicating that the engine encountered a hard start during the test. This trend was not observed in a previous test where the tank was partially filled, resulting in a thrust and pressure profile similar to the simulations.[34] The crossover between the tank and chamber pressure in the experimental data also suggests a recording error or anomaly occurring during the test.[34] Regardless, a similar trend is observed between the two data sets. The pressure profile in the P1B-Mk test showed better agreement (Figure 5). However, the experimental thrust curve shows highly oscillatory behaviour, indicating that the engine suffered combustion instabilities. The thrust curve used in this comparison is extracted from a filtered dataset[35] and shows some degree of agreement, despite the instabilities incurred. Test data from the HEROS 3 test-firing 6 demonstrated the best correspondence until the vapour phase transition. This suggests the engine was either shut off after liquid burnout or a

DOI: 10.13009/EUCASS2023-012

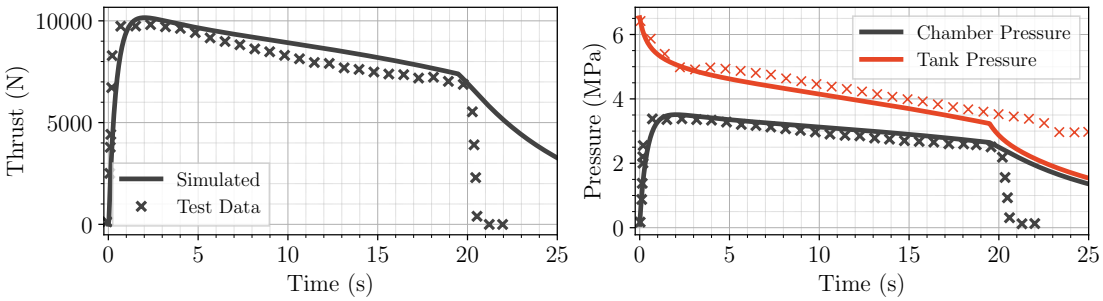

Figure 6: Validation of engine performance model against HEROS 3's test fire data[39]

.

different feed system or pressurisation method was employed. Overall, the model provides a viable prediction of the engine performance. However, further investigation is needed to improve the modelling of the vapour transition phase.

3.2 Geometry and Weight Estimation

The accuracy of the geometry and weight estimation module was also benchmarked against rocket specifications. Outputs of the engine sizing module with information on the vehicle's construction were used to predict the rocket's physical layout and estimate its weight. A scaled comparison between the generated geometry and the vehicle's physical configuration is provided in Figure 7. A comparison of the estimated vehicle specifications is provided in Table 1.

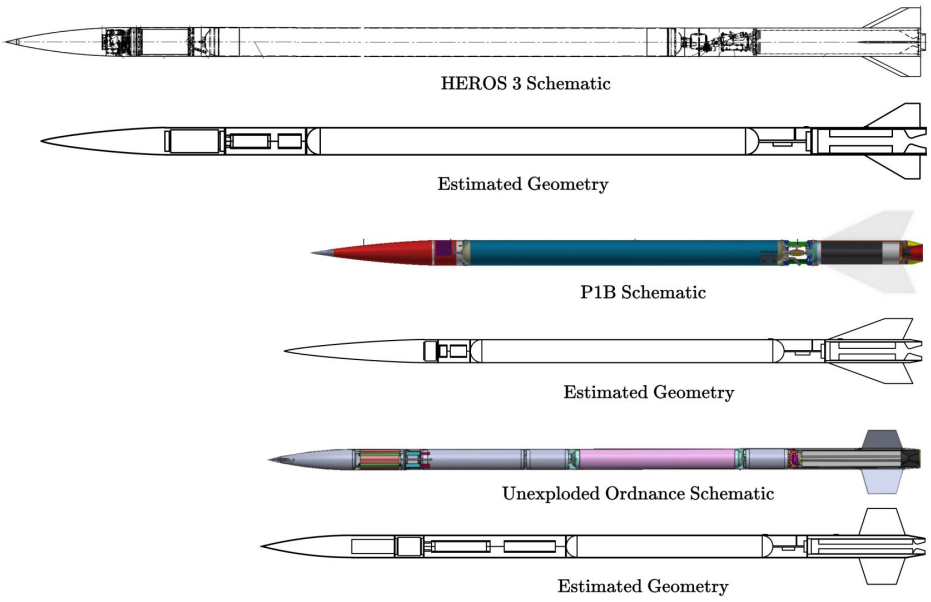

Figure 7: Comparison of output geometries with existing vehicle schematics.[34,36,38]

Relatively good estimates are found in all cases with margins of error within 10 %. This provides high confidence that the moment of inertia and centre of gravity estimates would also be reasonably predicted. One potential source of error in the results stems from incomplete information. As a result, underlying assumptions on several design and operational aspects, such as the tank ullage, had to be made to completely define all the inputs required for the geometry calculations and weight estimation. The only significant discrepancy observed was the fuel grain size predicted for the HEROS 3 vehicle, which was calculated to be 29 % shorter than the actual fuel grain despite being very similar in weight.[37] Since no information is provided on the fuel grain geometry or the type of paraffin wax used, it is hypothesised that one of these factors would have affected the prediction outcome.

DOI: 10.13009/EUCASS2023-012

Table 1: Summary of vehicle specification estimates.

Vehicle	**UXO**[34]			**P1B**[36]			**HEROS 3**[38]		
Parameters	**Estimated Value**	**True Value**	**Error %**	**Estimated Value**	**True Value**	**Error %**	**Estimated Value**	**True Value**	**Error %**
Vehicle Length	4.7	4.5	4.4	4.6	4.2	9.5	7.3	7.5	2.7
Propellant Mass	19.5	18.1	7.7	34.2	35.4	3.4	103	102	1.0
Vehicle Mass	43.3	46.7	7.3	38.3	40.7	5.9	70	75	6.7
Lift-Off Mass	62.8	64.9	3.2	72.5	76.1	4.7	173	177	2.3

3.3 Aerodynamics and Trajectory Simulation

Aerodynamics and trajectory both rely on external modules. As a result, the codes are not explicitly validated in this study but are tested in conjunction to ensure that the implementation in the framework is correct. Missile DATCOM has been used extensively in many vehicle design optimisation studies,[6,40,41] and its validity across a broad range of vehicle design configurations and flight profiles has been previously examined.[42–44] Comparative studies between DATCOM, CFD, and experimental data conducted by Nguyen[42,43] and Sooy[44] showed good agreement, making this an appropriate tool for aerodynamic prediction. RocketPy was also heavily validated during its development against a range of flight-proven sounding rockets.[28] A high degree of accuracy was demonstrated in these studies, with a maximum error of 4.2 % for estimated maximum velocity, 1.9 % for estimated apogee time, and 0.45 % for predicted apogee compared with recorded flight data.[28] A comparison of the integrated trajectory simulation with available flight data is provided in Figures 8-10, with a summary of the margins of error reported in Table 2.

Table 2: Summary of apogee prediction margin of errors.

Vehicle	**Predicted Apogee (m)**	**Recorded Apogee (m)**	**Error %**
UXO[34]	4209	4088 [a]	3.0
P1B[36]	18092	17900 [a]	1.1
HEROS 3[38]	32993	32300 [b]	2.1

[a] Above Ground Level, [b] Above Sea Level

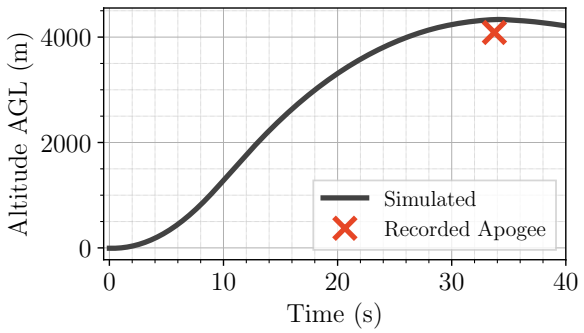

Figure 8: UXO simulated trajectory comparison.

Flight data was not publicly available for UXO's flight; however, the recorded apogee is provided and included in Figure 8. As presented in Figure 9, the simulated flight profile is compared to Balmogim's predicted flight profile modelled using the University of KwaZulu-Natal's 6-DOF code (HYROPS).[36,45] RocketPy predicted an apogee much closer to the actual value. Regardless of how closely aligned the altitude profiles appear, there is a considerable difference in the two modelled velocity profiles. Examination of the predictions made by Balmogim[35] and Broughton[36] found that the start-up thrust was predicted to be much higher than the test-firing data resulting in a steeper velocity profile. The HEROS 3 vehicle was the only project available in literature with complete flight data provided. The vehicle was initially designed to reach 40-50 km altitude; however, the launch rail was adjusted to 80° and the oxidiser tank was only filled to 70 % due to range safety requirements.[38] The model was adjusted to reflect these alterations.

DOI: 10.13009/EUCASS2023-012

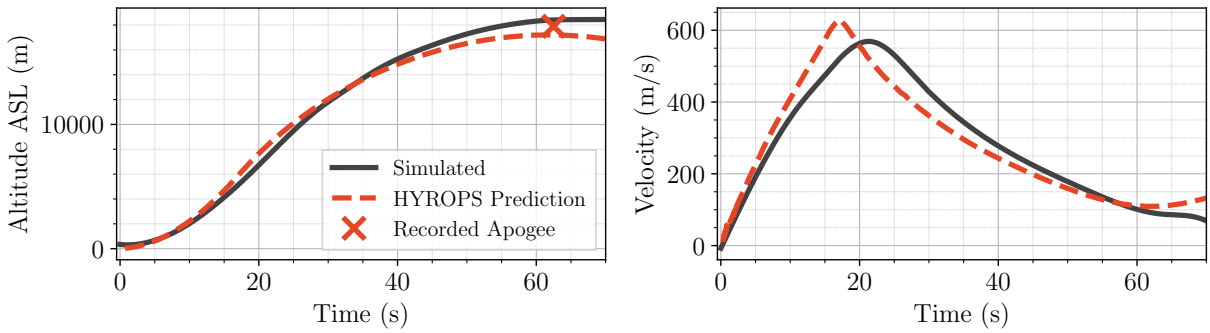

Figure 9: P1B simulated trajectory comparison.[36]

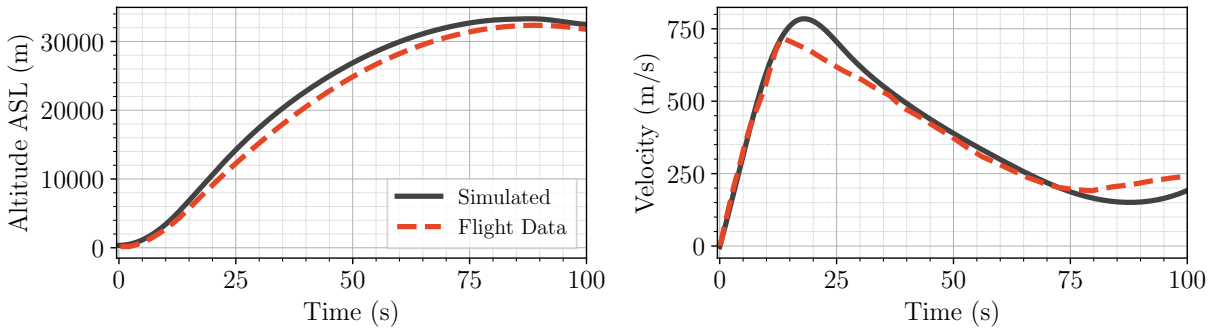

Figure 10: HEROS 3 simulated trajectory comparison.[38]

The simulation shows very good alignment with the test flight data during the initial ascent phase and begins to deviate after 15 seconds. The variations in the flight profile are attributed to the thrust curve at the vapour phase of the burn. The simulated thrust curve exhibits an exponential thrust decay. In contrast, the actual flight experiences a sharp drop in thrust, which is representative of an engine shut off, as shown in Figure 6. This explains why a sharp decrease in velocity is observed in the flight data while the simulated velocity continues to increase at a decreasing rate. As a result, the subsequent flight and apogee are slightly over-estimated. Regardless, the trajectory simulation still provides an acceptable estimation of the actual flight. As presented in this validation study, the results produced by Missile DATCOM and RocketPy show very good alignment with experimental data, indicating the modules have been integrated correctly.

As presented in this validation study, all modules provided physically plausible predictions. For instances where discrepancies arose, the difference in results was identified and explained. This shows that the simulation module is credible, making it sufficient for use in the optimisation framework.

4. Results

The design optimisation framework was applied to the conceptual design of a sub-orbital sounding rocket for carrying a CubeSat to an altitude of 100 km. The proposed vehicle serves as a technology demonstrator designed to deliver payloads to the Kármán Line for high altitude and micro-gravity space research. The rocket was designed using Paraffin (SASOL0907) as the fuel, Nitrous Oxide (N_2O) as the oxidiser and Nitrogen (N_2) as a pressurant. It uses a circular fuel port, combustion efficiency of 90 %, and 20 % tank ullage. A 10 m launch rail for initial guided ascent was used and Spaceport America was chosen as the launch site. A summary of the design variables and their limits is provided in Table 3. Payload weights between 0-25 kg were examined and the payload bay volume requirements were calculated assuming a 1U CubeSat form factor for each kilogram of payload.

The objectives are set to maximise the payload-to-propellant mass ratio. Constraints are applied to ensure that non-physical geometries are filtered out and additional design rules are applied. To ensure the vehicle reaches the Kármán Line, an inequality constraint for the simulated apogee is set between 100 km and 110 km. Similarly, to ensure the vehicle remains stable throughout flight, the vehicle must maintain a static margin between 1.5-6 body calibre

DOI: 10.13009/EUCASS2023-012

Table 3: Summary of optimisation input variables.

Design Variable	Lower Bound	Upper Bound	Design Variable	Lower Bound	Upper Bound
Payload Mass (kg)	0	25	Boat tail Convergence Ratio (d_b/d_f)	0.6	0.95
Peak Thrust (kN)	10	50	Boat tail Convergence Angle (°)	60	80
Burn Time (s)	10	50	Fin Sweep Angle (°)	10	75
Chamber Pressure (MPa)	2	4	Fin Root Chord Length (m)	0.25	2
Tank Pressure (MPa)	4.7	7	Fin Taper Ratio (% c_r)	0.05	1
OF Ratio	5	8.5	Fin Aspect Ratio (% c_r)	0.05	1.5
Body Diameter (m)	0.2	0.55	Fin Thickness (m)	0.001	0.025
Nose Cone Fineness Ratio (l_n/d_f)	2	6	Leading Edge Ratio (% c_t)	0.01	0.5
Nose Cone Power	0.25	1	Trailing Edge Ratio (% c_t)	0.01	0.5

during ascent and have a rail departure velocity above 30 m/s.[46] A minimum safety factor of 1.5 for fin flutter velocity is applied to ensure suitable fin geometries. The flutter velocity is given by:[47]

$$v_f = a\sqrt{\frac{G}{\frac{1.337AR^3P(\lambda+1)}{2(AR+2)\left(\frac{t}{c_r}\right)^3}}} \tag{6}$$

where G is the shear modulus, P is the atmospheric pressure, a is the speed of sound, AR is the aspect ratio, λ is the taper ratio, t is the thickness, and c_r is the root chord. Finally, geometry constraints were included to ensure the fins do not extend too far behind the rocket's body and that the boat tail does not clip into the nozzle. A summary of the optimisation problem is described below:

Objectives:

$$\text{maximise: } f_1(\mathbf{z}) = m_{payload}(\mathbf{z}) \tag{7}$$

$$\text{minimise: } f_2(\mathbf{z}) = m_{propellant}(\mathbf{z}) \tag{8}$$

Constraints:

$$h_{target} \leq h_{apogee}(\mathbf{z}) \leq 1.1h_{target} \tag{9}$$

$$min\Big(\frac{1}{d_{fus}}(x_{cp}(\mathbf{z},t) - x_{cg}(\mathbf{z},t))\Big) \geq 1.5 \tag{10}$$

$$max\Big(\frac{1}{d_{fus}}\Big(x_{cp}(\mathbf{z},t) - x_{cg}(\mathbf{z},t)\Big)\Big) \leq 6 \tag{11}$$

$$v(\mathbf{z},t) \leq 1.5v_f(\mathbf{z},t) \tag{12}$$

$$v_{depart}(\mathbf{z}) \geq v_{rail,min} \tag{13}$$

$$d_{base} \geq d_{noz} \tag{14}$$

$$x_{0,fins} + r_{span}tan(\theta_{sweep}) + c_t \leq l_{fuselage} + 2d_{fus} \tag{15}$$

4.1 Optimisation Results

The evolution of feasible solutions for this problem is presented in Figure 11 with a clear Pareto front produced. A near-linear trend between the payload capacity and the required propellant mass is observed. From the set of available solutions, designs with payload capacities of 5 kg increments were selected for further examination. A summary of the optimiser-selected parameters for these vehicles is outlined in Table 4 with the vehicle schematics presented in Figure 12.

As seen in the vehicle schematics, all rockets have similar profiles and vary by length based on the propellant requirements. The boat tail geometry, body diameter, and nose cone remain mostly consistent across all payload capacities.

4.2 HTPB Fuel Grain Substitution

A design study was conducted to examine the influence of the selected propellant combination on the vehicle design. Hydroxyl-terminated polybutadiene (HTPB), a synthetic rubber commonly used as a fuel for hybrid engines, was

DOI: 10.13009/EUCASS2023-012

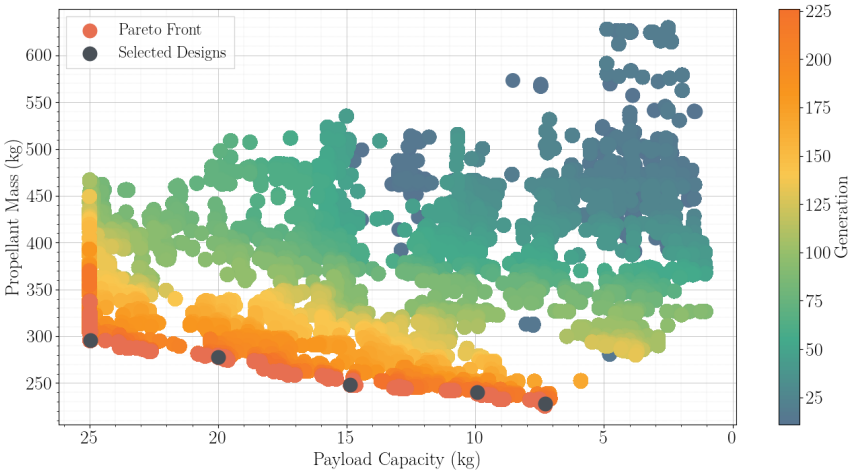

Figure 11: Pareto front for payload to propellant mass minimisation case.

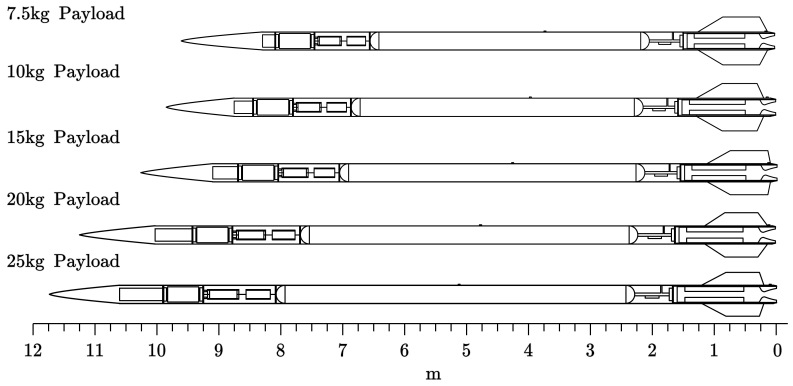

Figure 12: Comparison of vehicle schematics.

Table 4: Summary of selected design parameters.

Design Parameter	**7.3 kg**	**10 kg**	**15 kg**	**20 kg**	**25 kg**
Target Peak Thrust (kN)	22.21	23.17	23.44	27.02	27.28
Target Burn Time (s)	22.32	22.36	22.92	22.31	23.44
Chamber Pressure (MPa)	3.45	3.46	3.44	3.45	3.45
Tank Pressure (MPa)	5.23	5.24	6.24	4.76	5.28
OF Ratio	7.05	6.59	6.95	7.06	6.80
Body Diameter (m)	0.28	0.29	0.29	0.29	0.29
Nose Cone Fineness Ratio (l_n/d_f)	4.67	3.83	4.03	4.25	3.95
Nose Cone Power	0.67	0.69	0.75	0.75	0.67
Boat Tail Convergence Ratio (d_b/d_f)	0.92	0.94	0.95	0.92	0.95
Boat Tail Convergence Angle (°)	78.88	78.23	79.19	76.81	79.95
Fin Sweep Angle (°)	59.60	61.11	61.03	57.49	62.66
Fin Root Chord Length (m)	1.14	1.09	1.02	1.02	1.02
Fin Taper Ratio (% c_r)	0.53	0.52	0.59	0.52	0.53
Fin Aspect Ratio (% c_r)	0.21	0.21	0.20	0.20	0.20
Fin thickness (mm)	10.10	9.50	8.30	9.50	8.30
Leading Edge Ratio (% c_t)	0.30	0.19	0.27	0.25	0.27
Trailing Edge Ratio (% c_t)	0.49	0.32	0.47	0.49	0.30
Fin Tail Offset (m)	0.16	0.15	0.14	0.07	0.14

DOI: 10.13009/EUCASS2023-012

explored in this case.[48] HTPB has a significantly slower fuel regression rate than paraffin; however, its superior mechanical properties make it a desirable choice for large-scale engines with longer burn times.[49,50] In contrast, the poorer mechanical properties of paraffin make it prone to thermal degradation during prolonged motor firings affecting the overall scalability of the fuel grain. This issue is less severe for HTPB-based fuel grains due to its chemical composition.[49,50]

Initially, this case was run with the same settings as the previous optimisation case, with only the fuel type changing; however, the optimiser failed to size any vehicles capable of delivering a payload weight of 12 kg or above. The results showed that the lower fuel regression rate properties intrinsic to HTPB prohibited higher thrust (20 kN range) unless a high OF ratio was used. Increasing the oxidiser mass fraction to offset the reduced fuel mass flow rates leads to an extremely high total propellant mass requirement, rendering the option infeasible.

To compensate for the reduced regression rate, the fuel grain length has to be increased so that the burning surface area of the fuel port is large enough to deliver the required fuel mass flow rate. Consequently, this increases the volume of the combustion chamber, limiting the pressure build-up required for the engine to operate effectively. To overcome this issue, most HTPB/N_2O hybrid engines use a more effective grain geometry, such as a star or wagon wheel fuel port configuration, which increases the exposed surface area whilst minimising empty volume in the chamber. This design choice was implemented in the 75 kN engine of Spaceship One and Spaceship Two, which uses a multi-port configuration.[48] However, this is not completely necessary for high-performance oxidiser combinations such as HTPB/O_2 or HTPB/H_2O_2. For the secondary run, the circular fuel port is replaced with a 5-port star geometry and all other parameters remain the same. Figure 13 presents the results of the updated case with the previous limitation being effectively rectified. The payload capacity range now extends to the 25 kg defined upper limit. A comparison of the optimal vehicle designs, including the circular fuel port variations, is presented in Table 5 and Figure 14.

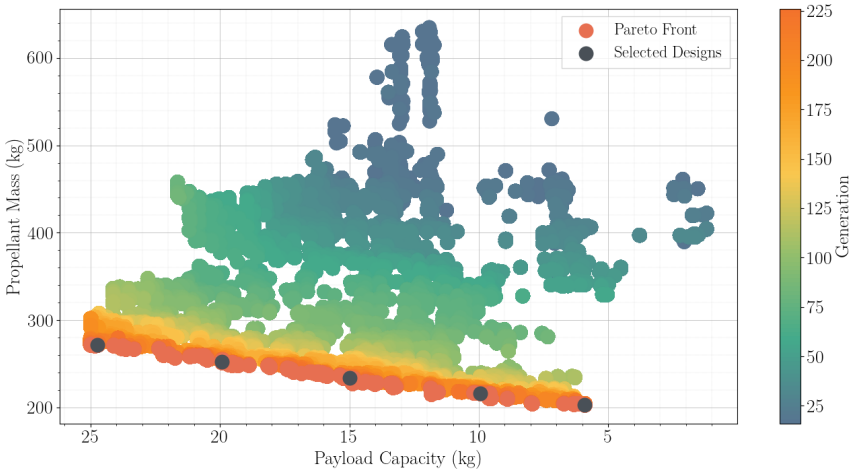

Figure 13: Pareto front for payload to propellant mass minimisation case using HTPB (star port geometry).

Star port fuel grains show a considerable improvement in volumetric efficiency compared to circular port grains, with up to a 15.6 % reduction in combustion chamber length and 4.95 % in overall length. However, this does not translate to a weight reduction as initially expected. The optimiser is limited by the maximum producible thrust of circular port grains and favours lower thrust engines with longer burn times. Consequently, this results in a lower thrust-to-weight ratio and rail departure velocity, impacting the vehicle's stability. The vehicles designed under a five star port geometry can achieve a much higher thrust-to-weight ratio and rail departure velocity.

Both configurations are designed with a propellant ratio less than the optimum OF ratio for HTPB/N_2O of 7.1. This is a trade-off selected by the optimiser to reduce the propellant tank size and weight. As expected, the OF ratio is higher for the circular port than the star port to compensate for the reduced fuel mass flux of the given configuration. In all cases, a tank pressure equivalent to the saturation pressure of N_2O is selected and the optimiser chooses not to include additional pressurising gas, which was not the case for the paraffin design study, because the OF ratio selected for HTPB/N_2O is substantially lower than paraffin/N_2O, translating to a lower oxidiser mass flow rate. The storage pressure of N_2O alone is enough to drive this flow without a pressurising gas. The reduced storage pressure also means the structural mass of the tank is reduced. This, combined with the lower oxidiser mass requirements, results in a lighter set of vehicles than the rockets propelled using paraffin/N_2O.

DOI: 10.13009/EUCASS2023-012

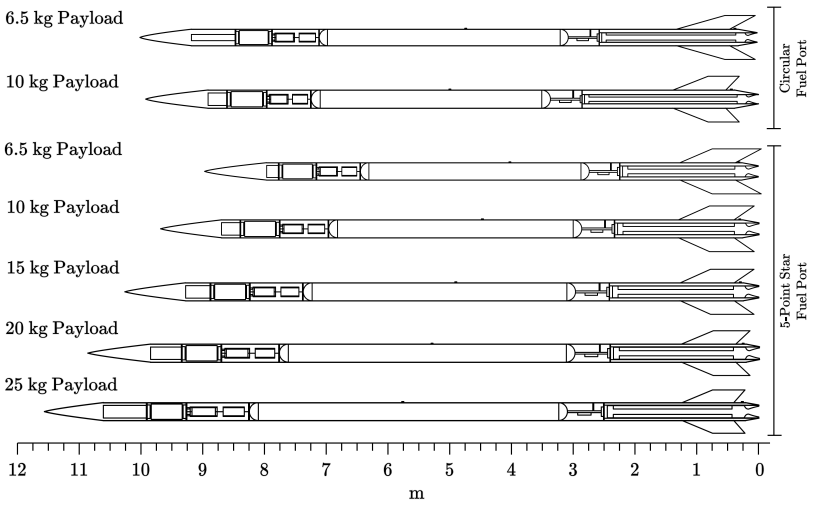

Figure 14: Comparison of vehicle schematics.

Table 5: Summary of selected design parameters.

Fuel Port Geometry	**Circular**		**5-Point Star**				
Design Parameter	**6.5 kg**	**10 kg**	**6.5 kg**	**10 kg**	**15 kg**	**20 kg**	**25 kg**
Target Peak Thrust (kN)	14.43	16.72	21.13	19.93	21.49	21.05	22.68
Target Burn Time (s)	24.75	25.55	20.38	22.28	22.88	25.14	25.13
Chamber Pressure (MPa)	2.89	3.05	3.11	3.16	3.16	3.04	3.04
Tank Pressure (MPa)	4.72	4.72	4.72	4.71	4.77	4.71	4.71
OF Ratio	6.45	6.44	5.07	5.01	5.03	5.02	5.02
Body Diameter (m)	0.26	0.28	0.29	0.29	0.29	0.29	0.29
Nose Cone Fineness Ratio (ln/df)	0.32	0.35	0.38	0.35	0.35	0.36	0.33
Nose Cone Power	0.70	0.72	0.77	0.78	0.78	0.79	0.78
Boat Tail Convergence Ratio (d_b/d_f)	0.80	0.78	0.85	0.90	0.83	0.87	0.87
Boat Tail Convergence Angle (°)	75.29	79.91	0.80	0.80	0.80	0.79	0.80
Fin Sweep Angle (°)	74.29	68.91	67.62	66.52	66.26	67.63	62.66
Fin Root Chord Length (m)	0.85	0.85	0.94	0.91	0.88	0.86	0.84
Fin Taper Ratio (% c_r)	0.57	0.59	0.86	0.81	0.81	0.67	0.63
Fin Aspect Ratio (% c_r)	0.26	0.26	0.25	0.25	0.25	0.24	0.24
Fin thickness (mm)	9.03	9.91	8.89	8.39	8.38	8.21	8.23
Leading Edge Ratio (% c_t)	0.29	0.29	0.32	0.24	0.24	0.25	0.32
Trailing Edge Ratio (% c_t)	0.38	0.39	0.40	0.42	0.42	0.44	0.37
Fin Tail Offset (m)	0.02	0.13	0.02	0.03	0.14	0.17	0.18

4.3 Comparison and Verification of Vehicle Designs

A comparison of the vehicle designs under each propellant combination is presented. More specifically, the 10 kg and 25 kg payload capacity vehicles are examined and this is compared to NAMMO's Nucleus vehicle, which successfully launched to 107 km in 2018.[51] Figure 15 compares the vehicle schematics with the specifications outlined in Table 6.

As presented in Table 6, the difference in total length, propellant mass, and gross lift-off mass can be seen. HTPB/N_2O and paraffin/N_2O both have very comparable optimum characteristic velocities ($c^*_{\text{HTPB/N}_2\text{O}}$ =1604.5 m/s, $c^*_{\text{paraffin/N}_2\text{O}}$ =1605.7 m/s) and specific impulses ($I_{sp,\text{HTPB/N}_2\text{O}}$ =247 m/s, $I_{sp,\text{paraffin/N}_2\text{O}}$ =248 m/s). The OF ranges where these optima exist, however, vary significantly. These differences are reflected in the vehicle designs. Additionally, the schematics illustrate how each propellant combination's fuel regression rate affects the propulsion system's design. The HTPB combustion chamber has a significantly higher aspect ratio than the paraffin chamber, which is much more compact due to the higher fuel regression rate. As discussed earlier, the lower optimum OF ratio of the HTPB/N_2O means that less propellant and a lower tank pressure is required, resulting in a lighter vehicle overall. HTPB has a much lower fuel regression rate and once this issue is addressed, with improvements in the fuel grain geometry, HTPB becomes a much more effective fuel.

DOI: 10.13009/EUCASS2023-012

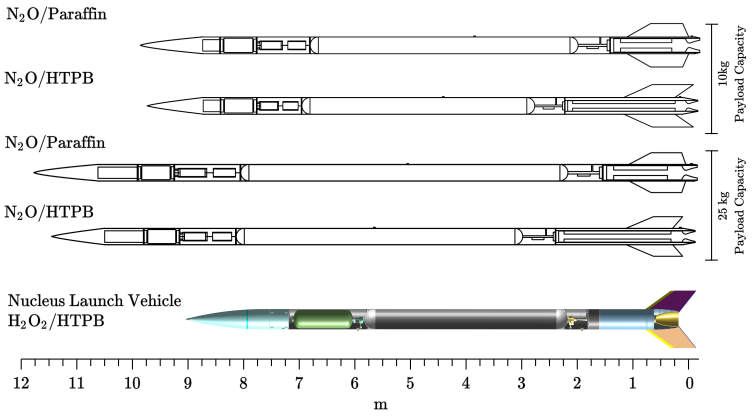

Figure 15: Comparison of propellant selection on vehicle design.

Table 6: Comparison of vehicle specifications.

Payload Capacity	**10 kg**		**25 kg**		**62 kg**[51]
Propellant Combination	**N_2O /Paraffin**	**N_2O /HTPB**	**N_2O /Paraffin**	**N_2O /HTPB**	**H_2O_2 /HTPB**
Total Length (m)	9.84	9.77	11.80	11.61	9.0[51]
Body Diameter (m)	0.29	0.29	0.29	0.29	0.36[51]
Vehicle Weight (kg)	156.31	128.00	201.89	168.91	-
Propellant Weight (kg)	240.11	216.19	295.59	271.92	-
Lift-Off Weight	396.42	344.19	497.48	440.82	815[51]
Peak Thrust (kN)	23.21	20.03	27.07	21.31	30[51]
Total Burn Time (s)	35.19	37.65	35.16	40.61	> 39[51]

The optimiser has sized all vehicles to a scale similar to the Nucleus vehicle and the discrepancies can be explained by the design choices made for this particular rocket. Despite having a payload capacity of 62 kg, the rocket is much more compact as it does not have a recovery system.[51] The Nucleus vehicle is also substantially heavier than the ones sized by the optimiser as it uses a complete aluminium construction instead of carbon fibre.[51] This also explains why a higher thrust of 30 kN was selected. The choice of HTPB/H_2O_2 as the propellant also reduces the aspect ratio of the propulsion system. A considerably lower OF ratio is required to achieve optimum combustion performance when compared to using N_2O as the oxidiser. The better overall performance meant that a more compact combustion chamber could be used and the lower optimal OF ratio meant less oxidiser was required. The combustion chamber diameter most likely governed the airframe diameter in this vehicle. This is 25 % larger than the ones the optimiser chose, explaining the reduction in overall length compared to the design options deduced in this study. This effectively illustrates the impact that the choice of propellant has on the vehicle design whilst confirming that the results of the optimiser are credible.

5. Conclusion

A framework was developed for the medium-fidelity multidisciplinary design optimisation of hybrid rockets, thus addressing the shortcomings of current optimisation approaches by improving the simulation fidelity while maintaining a large design space. The model was validated with experimental data available in the literature and showed good agreement across all disciplines. As noted, the propulsion simulation needs additional work to address the vapour transition phase of the burn. The code was applied to a 100 km sub-orbital class rocket design study proposed for high-altitude scientific research. In this investigation, a set of optimal vehicle designs were derived and explored, with the effect of the choice of propellant and fuel grain geometry investigated. It was found that hybrid launch vehicles suffer from poor volumetric efficiencies and scaling issues compared to liquid and solid equivalent vehicles. Furthermore, despite its poorer regression rate, the use of HTPB results in a lighter and more compact vehicle than paraffin. Additionally, HTPB becomes less feasible at high thrust ranges unless an optimised fuel port geometry with a larger burning surface area is used. Overall, the design tool fulfilled the requirements and provided an adequate foundation for further expansion.

DOI: 10.13009/EUCASS2023-012

References

[1] M. Smiley, M. Veno, and R. Bell. Commercial crew development-round one, milestone 3: Overview of sierra nevada corporation's hybrid motor ground test. *47th AIAA/ASME/SAE/ASEE Joint Propulsion Conference and Exhibit*, 2011.

[2] Shimada T. Status summary of fy 2011 hybrid rocket research working group. *Ninth International Conference on Flow Dynamics, Sendai, Japan*, 2014.

[3] Ashley C. Karp, Barry Nakazono, Joel Benito Manrique, Robert Shotwell, David Vaughan, and George T. Story. A hybrid mars ascent vehicle concept for low temperature storage and operation. *52nd AIAA/SAE/ASEE Joint Propulsion Conference*, 2016.

[4] Lorenzo Casalino, Francesca Letizia, and Dario Pastrone. Design trade-offs for hybrid rocket motors. *48th AIAA/ASME/SAE/ASEE Joint Propulsion Conference and Exhibit*, 2012.

[5] Mehmet Burak Ozbilgin, H. Telli, and O. Ozkan. Hybrid rocket engine design with multi-objective vibrational genetic algorithm. *2017 8th International Conference on Recent Advances in Space Technologies (RAST)*, pages 61–66, 2017.

[6] Francisco Miranda, Dominic Dirkx, and B.T.C Zandbergen. Design optimisation of ground and air launched hybrid rockets. *66th International Astronautical Congress,*, 2012.

[7] Hao Zhu, Hui Tian, Guobiao Cai, and Weimin Bao. Uncertainty analysis and design optimization of hybrid rocket motor powered vehicle for suborbital flight. *Chinese Journal of Aeronautics*, 28(3):676–686, 2015.

[8] Hao Zhu, Pengcheng Wang, Weile Xu, Yuanjun Zhang, Hui Tian, and Guobiao Cai. Design optimization and parameter analysis of a hybrid rocket motor-powered small leo launch vehicle. *International Journal of Aerospace Engineering*, 2021:1–20, 2021.

[9] Pedro Luiz Kaled Da Cás, Cristiano Queiroz Vilanova, Manuel Nascimento Dias Barcelos Jr, and Carlos Alberto Gurgel Veras. An optimized hybrid rocket motor for the sara platform reentry system. *Journal of Aerospace Technology and Management*, 4(3):317–330, 2012.

[10] M. Kanazakia, A. Ariyairt, K. Chiba, and K. Kitagawa. Conceptual design of single-stage rocket using hybrid rocket by means of genetic algorithm. *2014 Asia-Pacific International Symposium on Aerospace Technology,APISAT2014*, 2014.

[11] DaLin Rao, GuoBiao Cai, Hao Zhu, and Hui Tian. Design and optimization of variable thrust hybrid rocket motors for sounding rockets. *Science China Technological Sciences*, 55(1):125–135, 2011.

[12] D. J. Vonderwell, I. F. Murray, and S. D. Heister. Optimization of hybrid-rocket-booster fuel-grain design. *Journal of Spacecraft and Rockets*, 32(6):964–969, 1995.

[13] M. B Anderson. *Design of a Missile Interceptor Using a Genetic Algorithm*. PhD thesis, Dissertation, Aerospace Engineering Department,Auburn University, 1998.

[14] Douglas J. Bayley, Roy J. Hartfield, John E. Burkhalter, and Rhonald M. Jenkins. Design optimization of a space launch vehicle using a genetic algorithm. *Journal of Spacecraft and Rockets*, 45(4):733–740, 2008.

[15] Ahmed Mahjub, Nurul Musfirah Mazlan, M. Z. Abdullah, and Qummare Azam. Design optimization of solid rocket propulsion: A survey of recent advancements. *Journal of Spacecraft and Rockets*, 57(1):3–11, 2020.

[16] F.K Leverone. Performance modelling and simulation of a 100km hybrid sounding rocket. Master's thesis, Mechanical Engineering, College of Agriculture, Engineering and Science, 2013.

[17] B.J. McBride and S. Gordon. Computer program for calculation of complex chemical equilibrium compositions and applications i. analysis. *NTRS - NASA Technical Reports Server*, 1996.

[18] B.J. McBride and S. Gordon. Computer program for calculation of complex chemical equilibrium compositions and applications ii. users manual and program description. *NTRS - NASA Technical Reports Server*, 1996.

[19] R. W. Humble, G. N. Henry, and W. J. Larson. *Space Propulsion Analysis and Design*. McGraw-Hill Book Company, 2007.

[20] B. Genevive. Development of a hybrid sounding rocket motor. Master's thesis, Mechanical Engineering, College of Agriculture, Engineering and Science, 2013.

[21] B. Genevive, de la Beaujardiere P., and M.J Brooks. A computational tool for predicting hybrid rocket motor performance. *R&D Journal of the South African Institution of Mechanical Engineering*, page 56â65, 2017.

[22] S. Borgdorff. Nitrous oxide state estimation in hybrid rocket oxidizer tanks. Master's thesis, 2017.

[23] Jonathan Mcculley, Andrew Bath, and Stephen Whitmore. Design and testing of fdm manufactured paraffin-abs hybrid rocket motors. *48th AIAA/ASME/SAE/ASEE Joint Propulsion Conference and Exhibit*, 2012.

[24] Teodor-Viorel Chelaru and Florin Mingireanu. Hybrid rocket engine, theoretical model and experiment. *Acta Astronautica*, 68(11-12):1891â1902, 2011.

[25] G Marxman and M Gilbert. Turbulent boundary layer combustion in the hybrid rocket. In *Symposium (International) on Combustion*, volume 9, pages 371–383. Elsevier, 1963.

DOI: 10.13009/EUCASS2023-012

[26] E. L. Fleeman and J. A. Schetz. *Missile Design and System Engineering*. American Institute of Aeronautics and Astronautics, 2012.

[27] S. R. Vukelich, S. L. Stoy, K. A. Burns, Castillo J. A., and Moore M. E. *Missile DATCOM. Volume 1.* McDonnell Douglas Missile Systems Co., St. Louis, MO.; Air Force Wright Aeronautical Labs., Wright-Patterson AFB, OH., 1988.

[28] Giovani H. Ceotto, Rodrigo N. Schmitt, Guilherme F. Alves, Lucas A. Pezente, and Bruno S. Carmo. Rocketpy: Six degree-of-freedom rocket trajectory simulator. *Journal of Aerospace Engineering*, 34(6), 2021.

[29] W. T. Thomson and G. S. Reiter. Jet damping of a solid rocket - theory and flight results. *AIAA Journal*, 3(3):413â417, 1965.

[30] William T. Thomson. Equations of motion for the variable mass system. *AIAA Journal*, 4(4):766â768, 1966.

[31] K. Deb, A. Pratap, S. Agarwal, and T. Meyarivan. A fast and elitist multiobjective genetic algorithm: Nsga-ii. *IEEE Transactions on Evolutionary Computation*, 6(2):182â197, 2002.

[32] David Riddle, Roy Hartfield, John Burkhalter, and Rhonald Jenkins. Genetic algorithm optimization of liquid propellant missile systems. *45th AIAA Aerospace Sciences Meeting and Exhibit*, 2007.

[33] Irina Bolodurina and Lyubov Zabrodina. Investigation of optimization algorithms for neural network solutions of optimal control problems with mixed constraints. *Machines*, 9(5):102, 2021.

[34] University of Waterloo. Unexploded ordnance hybrid rocket,team 38 project technical report for the 2018 irec. *Experimental Sounding Rocket Association - Spaceport America Cup Technical Reports*, 2018.

[35] U. Balmogim. Design and development of the phoenix-1b hybrid rocket. Master's thesis, Mechanical Engineering, College of Agriculture, Engineering and Science, 2017.

[36] K.M Brouhgton. motor design for a sub-orbtital hybrid rocket. Master's thesis, Mechanical Engineering, College of Agriculture, Engineering and Science, 2018.

[37] M. Kobald, C. Schmierer, U. Fischer, K. Tomilin, A. Petrarolo, and M. Rehberger. The hyend stern hybrid sounding rocket project. *Progress in Propulsion Physics â Volume 11*, 2019.

[38] Mario Kobald, Christian Schmierer, Ulrich Fischer, Konstantin Tomilin, and Anna Petrarolo. A record flight of the hybrid sounding rocket heros 3. *Transactions Of The Japan Society For Aeronautical And Space Sciences, Aerospace Technology Japan*, 16(3):312â317, 2018.

[39] Mario Kobald, Ulrich Fischer, Konstantin Tomilin, Anna Petrarolo, Paula Kysela, Christian Schmierer, Andreas Pahler, Jonas Gauger, Jonas Breitinger, Ferdinand Hertel, and et al. Sounding rocket "heros" - a low-cost hybrid rocket technology demonstrator. *53rd AIAA/SAE/ASEE Joint Propulsion Conference*, 2017.

[40] J.D Vasile, J.T. Bryson, and Fresconi F.E. Aerodynamic design optimization of long-range projectiles using missile datcom. *AIAA Scitech 2020 Forum*, 2020.

[41] H. Villanueva1, F.M.and Linshu and X Dajun. Small solid propellant launch vehicle mixed design optimization approach. *Journal of Aerospace Technology and Management*, 2014.

[42] Nhu Van Nguyen, Maxim Tyan, Sunghyun Jin, and Jae-Woo Lee. Adaptive multifidelity constraints method for efficient multidisciplinary missile design framework. *Journal of Spacecraft and Rockets*, 53(1):184â194, 2016.

[43] Nhu-Van Nguyen, Maxim Tyan, Jae-Woo Lee, and Yung-Hwan Byun. Investigations on missile configuration aerodynamic characteristics for design optimization. *Transactions Of The Japan Society For Aeronautical And Space Sciences*, 57(4):210â218, 2014.

[44] Thomas Sooy and Rebecca Schmidt. Aerodynamic predictions, comparisons, and validations using missile datcom and aeroprediction 98 (ap98). *42nd AIAA Aerospace Sciences Meeting and Exhibit*, 2004.

[45] Seffat Chowdhury, Jean Pitot De La Beaujardiere, Michael Brooks, and Lance Roberts. An integrated six degree-of-freedom trajectory simulator for hybrid sounding rockets. *49th AIAA Aerospace Sciences Meeting including the New Horizons Forum and Aerospace Exposition*, 2011.

[46] Experimental Sounding Rocket Association. Intercollegiate rocket engineering competition design, test, and evaluation guide, 2023.

[47] M.J. Martin. Summary of flutter experiences as a guide to the preliminary design of lifting surfaces on missiles. *Technical Report NACA TN 4197*, 1958.

[48] Martin J Chiaverini. *Fundamentals of Hybrid Rocket Combustion and Propulsion*. American Institute of Aeronautics and Astronautics, 2007.

[49] J.C Thomas, J.M Stahl, Tykol A.J, F.A Rodriguez, and E.L2 Petersen. Hybrid rocket studies using htpb/paraffin fuel blends in gaseous oxygen flow. *7th European Conference for Aeronautics and Space Sciences*, 2017.

[50] Arif M. Karabeyoglu and Ugur Arkun. Evaluation of fuel additives for hybrid rockets and sfrj systems. *50th AIAA/ASME/SAE/ASEE Joint Propulsion Conference*, 2014.

[51] Martina Faenza, Adrien J. Boiron, Bastien Haemmerli, and Constans J. Verberne. The nammo nucleus launch: Norwegian hybrid sounding rocket over 100km. *AIAA Propulsion and Energy 2019 Forum*, 2019.